Determination of the Capacitance of Solid-State Potentiometric Sensors: An Electrochemical Time-of-Flight Method

Heather A. Elsen, Katarzyna Slowinska,† Ewa Hull,‡ and Marcin Majda*

Department of Chemistry, University of California, Berkeley, Berkeley, California 94720-1460

A dual microelectrode electrochemical time-of-flight technique in which diffusion flux of Ag^+, Cl^-, or H^+ ions electrochemically produced at a generator electrode is measured by recording potential−time transients with Ag, Ag/AgCl, or iridium oxide potentiometric microsensors, respectively, is developed. The generator and microsensor electrodes are typically spaced by 50−100 μm and are incorporated in the lithographically fabricated thin-layer-type devices. Under conditions of moderate rates of the ion electrogeneration, the potential−time ($E-t$) transients recorded with the three microsensors show excellent agreement with theory involving linear diffusion equations and the experimentally determined Nernstian slopes of the microsensors. However, when the generator current, or the initial concentration of the primary ion of interest is low, appreciable delays in the recorded $E-t$ transients are observed due to the finite capacitance of the micropotentiometric sensors. The recorded delay in the $E-t$ transients can be quantitatively accounted for by including the sensor capacitance (C) in the theoretical description of the transients. Direct comparison between the theoretical and the experimental $E-t$ transients yields the sensor's capacitance. This capability of our new technique is unique in that it allows determination of the capacitance of a potentiometric sensor at open circuit. In the cases of silver electrodes, this method results in $C = 31 \pm 2$ μF/cm², a value that is in agreement with those obtained by other methods. The results for silver chloride sensors yield a C in the range of 100−140 ± 10 μF/cm². The specific values depend on sensor preparation and the resulting roughness of the Ag/AgCl interface. Iridium oxide sensors show a capacitance that linearly depends on the thickness of the film. Specific capacitance of these microporous films was determined to be 59 ± 6 F/cm³.

As micropotentiometric sensors find an increasing range of applications in biological sciences and medicine and as components of modern analytical measurement techniques,[1−7] it is necessary to fully characterize all their operating parameters. Most studies explore the sensitivity and selectivity. Some, in addition, determine sensor response time.[8−15] However, it becomes increasingly important to also characterize capacitance in order to optimize the microsensor's performance. In applications involving very small sample volumes, such as those relying on microfluidic devices, or involving low analyte concentrations, sensor capacitance can be performance-limiting.[16−18]

When dealing with characterization of potentiometric sensors, the effect of capacitance is not one commonly considered. Although the importance of both ion selectivity and sensitivity are widely understood, the effect of sensor capacitance is not. In the process of sensor equilibration in an analyte solution involving a change of sensor's potential, some of the ions generating a sensor's selective response are consumed (or generated). Depending on the type of potentiometric sensor, this may involve either an electron transfer or an ion-exchange reaction at the sensor surface. For example, an increase in silver ion activity near a silver potentiometric sensor results, at open circuit, in a net reduction of silver ions at the sensor surface, thus leading to an increase in the sensor potential. Likewise, an increase in a solution's proton activity, provoking an increase in the potential of a pH sensor immersed in that solution is a direct result of a shift of the proton exchange equilibrium at the sensor surface that reduces proton activity on the solution side of the interface. Regardless of the nature of the equilibration reaction, the relationship between the sensor potential and activity of the primary ion

* Corresponding author. Fax: (510) 642-0269. E-mail: majda@berkeley.edu.

† Permanent address: Department of Chemistry and Biochemistry, California State University, Long Beach, CA 90840.

‡ Permanent address: Department of Materials Science and Ceramics, University of Science and Technology, 30-059 Krakow, Poland.

(1) Lindner, E.; Buck, R. P. *Anal. Chem.* **2000**, *72*, 336A.
(2) Lauks, I. R. *Acc. Chem. Res.* **1998**, *31*, 317.
(3) Mailly, S. C.; Hyland, M.; Mailley, P.; McLaughlin, J. M.; McAdams, E. T. *Mater. Sci. Eng.* **2001**, *21*, 167.
(4) Spaine, T. W.; Baur, J. E. *Anal. Chem.* **2001**, *73*, 930.
(5) Wipf, D. O.; Ge, F.; Spaine, T. W.; Baur, J. E. *Anal. Chem.* **2000**, *72*, 4921.
(6) Marzouk, S. A. M.; Ufer, S.; Buck, R. P.; Johnson, T. A.; Dunlap, L. A.; Cascio, W. E. *Anal. Chem.* **1998**, *70*, 5054.
(7) Wei, C.; Bard, A. J.; Nagy, G.; Toth, C. *Anal. Chem.* **1995**, *67*, 1346.
(8) Rechnitz, G. A. *Talanat* **1964**, *11*, 1467.
(9) Johansson, G.; Norberg, K. *J. Electroanal. Chem.* **1968**, *18*, 239.
(10) Toth, K.; Gavaller, I.; Pungor, E. *Anal. Chim. Acta* **1971**, *57*, 131.
(11) Toth, K.; Pungor, E. *Anal. Chim. Acta* **1973**, *64*, 417.
(12) Mertens, J.; Van den Winkel, P.; Massart, D. L. *Anal. Chem.* **1976**, *48*, 272.
(13) Yao, S.; Wang, M.; Madau, M. *J. Electrochem. Soc.* **2001**, *148*, H29.
(14) Lindner, E.; Toth, K.; Pungor, E.; Berube, T. R.; Buck, R. P. *Anal. Chem.* **1987**, *59*, 2213.
(15) Slowinska, K.; Majda, M. *J. Solid State Electrochem.* **2004**, *8*, 763−771.
(16) Suzuki, H.; Shiroishi, H.; Sasaki, S.; Karube, I. *Anal. Chem.* **1999**, *71*, 5069.
(17) Satoh, W.; Hosono, H.; Suzuki, H. *Anal. Chem.* **2005**, *77*, 6857.
(18) Ges, I. G.; Ivanov, B. L.; Schaffer, D. K.; Lima, E. A.; Werdich, A. A.; Baudenbacher, F. J. *Biosens. Bioelectron.* **2005**, *21*, 248.

10.1021/ac060449w CCC: $33.50
Published on Web 08/12/2006

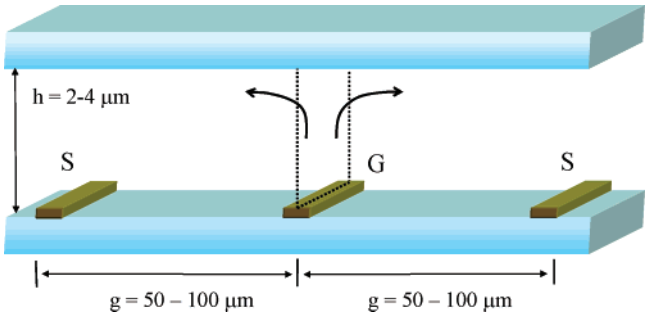

Figure 1. A schematic drawing of the main components of a narrow-channel, electrochemical time-of-flight device. The generator electrode (G) and the two symmetrically positioned sensor electrodes (S) are lithographically fabricated on a glass slide. A second, parallel glass slide is located at a distance, h, of ~2−4 μm from the electrode assembly. Typical spacing between the generator and the sensor is g of 50−100 μm.

is governed by the Nernst equation. In turn, the differential quantity of ions involved in such equilibria is proportional to the sensor capacitance. Therefore, as we document below, the very equilibrium leading to the establishment of the sensor potential may alter the concentration of the analyte one intends to measure. In cases in which potentiometric sensors are used to monitor changes in the activity of a particular ion, the phenomena outlined above may also lead to an apparent delay in the sensor's response even if the sensor intrinsic response kinetics are very fast.[15,19] We discuss this at a greater length below.

We take advantage of these phenomena to develop a new technique capable, for the first time, of determining the capacitance of a potentiometric sensor at open circuit. The method relies on a controlled perturbation of the activity of the primary ion in a small volume adjacent to the sensor surface. The observed delay in a sensor response relative to the predictions based on an assumption of negligible surface capacitance is then interpreted to yield the sensor's capacitance. It is important to stress that unlike classical methods of measuring interfacial capacitance that rely on the application of a potential or current perturbation to an electrode of interest, our method is unique in that it involves, instead, open circuit potential measurements of an electrode of interest in response to a controlled perturbation of the activity of its primary ion.

P-ETOF, potentiometric electrochemical time-of-flight is a new method in which potential−time ($E-t$) transients of a solid-state microsensor are recorded in response to an increasing concentration of the primary ions using a lithographically fabricated dual-microelectrode device shown schematically in Figure 1. The two microband electrodes are situated in close proximity (50−100 μm). One electrode is used to electrochemically generate species of interest, such as Ag^+, Cl^-, or H^+. The generator electrode operates under galvanostatic or constant rate conditions. The other microband electrode is the potentiometric microsensor exhibiting a Nernstian response with respect to the generated ions. We used Ag, Ag/AgCl, and IrO_2 as the microsensors. The method outlined here is analogous to the original amperometric time-of-flight technique introduced by Feldman et al.[23] and used by others to measure diffusion constants of redox species.[21−25] However, unlike the amperometric time-of-flight technique, P-ETOF uses the constant current generation and potentiometric sensing first described in our previous reports.[15,19]

As shown in Figure 1, the two microband electrodes are confined to a narrow channel of ~3 μm between the device surface and a second glass cover slip. Au counter and Ag reference electrodes are also confined to the narrow channel but not shown in this schematic. Since the thickness of the narrow channel in this sandwich device is far smaller than the interelectrode gap (g), the diffusion of the electrogenerated ions in the channel between the generator and sensor microelectrodes obeys linear diffusion equations. Specifically, we can solve Fick's diffusion equations to obtain the following expression for the time-dependent concentration of the diffusing ions at the sensor microelectrode, $C(g,t)$,[26]

$$C(g,t) = C_{\text{in}} + \frac{i}{nFAD}\left\{2\left(\frac{Dt}{\pi}\right)^{1/2}\exp\left(-\frac{g^2}{4Dt}\right) - g \times \operatorname{erfc}\left[\frac{g}{2(Dt)^{1/2}}\right]\right\} \quad (1)$$

where C_{in} and D are the initial, background concentration of the ions in the channel and their diffusion constant, F is Faraday's constant, and i is the value of the constant current applied to generate the ions (50% value of the applied current is used, since the symmetric design of the device results in just 50% of the generated ions diffusing toward one of the microsensors electrodes). A, the effective surface area of the generator microelectrode is taken as the cross-sectional area of the narrow channel equal to the product of the length (l) of the microband electrodes and the height (h) of the channel. The linear diffusion approximation mentioned above allows us to treat the generator electrode as if it were occupying the entire cross-sectional area of the narrow channel, as shown in Figure 1. The height of the narrow channel is established by the polymeric spacers (see the Experimental Section). Equation 1, combined with the Nernst equation and the value of the experimentally determined Nernstian slope, is used to predict the shapes of the $E-t$ transients recorded in the P-ETOF experiments. We show that the comparison of the predicted and recorded $E-t$ transients can be used to obtain the capacitance of the microsensors.

In this report, we first describe the functioning of our P-ETOF method using silver and Ag/AgCl microband electrodes both to generate and potentiometrically to sense silver and chloride ions, respectively. Next, we outline conditions under which a delay in the rise of the sensor's potential can be observed relative to the theoretical expectations. The delay in the $E-t$ transients is used

(19) Slowinska, K.; Feldberg, S. W.; Majda, M. *J. Electroanal. Chem.* 2003, *554−555*, 61.
(20) Feldman, B. J.; Feldberg, S. W.; Murray, R. W. *J. Phys. Chem.* **1987**, *91*, 6558.
(21) Licht, S.; Cammarata, V.; Wrighton, M. S. *Science* **1989**, *243*, 1176.
(22) Cammarata, V.; Talham, D. R.; Crooks, R. M.; Wrighton, M. S. *J. Phys. Chem.* **1996**, *94*, 2680.
(23) Licht, S.; Cammarata, V.; Wrighton, M. S. *J. Phys. Chem.* **1990**, *94*, 6133.
(24) Tatistcheff, H. B.; Fritsch-Faules, I.; Wrighton, M. S. *J. Phys. Chem.* **1993**, *97*, 2732.
(25) Wittek, M.; Möller, G.; Johnson, M. J.; Majda, M. *Anal. Chem.* **2001**, *73*, 870.
(26) Bard, A. J.; Faulkner, L. R. *Electrochemical Methods. Fundamentals and Applications*, 2nd ed.; J. Wiley & Sons: New York, 2001; Chapter 8, pp 305−310.

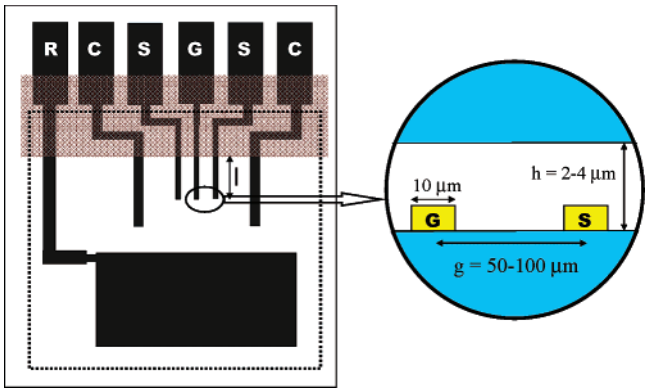

Figure 2. A schematic drawing of the entire narrow-channel time-of-flight device electrode assembly (left) and a cross section of the generator and sensor pair (right). The reference electrode (R) is silver-plated in all experiments. The two counter electrodes (C) are externally shorted. Alhough the generator electrode (G) is flanked by two sensor electrodes (S), only one of those is used in each experiment. An ~1-μm-thick layer of an inert polymer, shown as the shaded area, is used to isolate the working section of the electrodes from their contact area. The polymer film also defines the length (l = 2.0 mm) of the generator and sensor electrodes. The dotted line outlines the size and the position of the top glass slide used to form the narrow channel filled with electrolyte solution above the electrode assembly plate. Four small polymeric spacers (not shown in the figure) are deposited in each corner of the top glass slide to define the thickness of the narrow channel.

to determine the sensor's capacitance. Using this approach, we then measure the capacitance of the Ag, Ag/AgCl, and IrO_2 microsensors. Whereas in the case of the silver sensor, the capacitance can be measured using standard electrochemical methods, in the other two cases, this is far less straightforward. In fact, data presented below offer new insight into the properties of these microsensors. Specifically, in the case of the IrO_2 sensors, we show that the capacitance is proportional to their volume, confirming the existence of appreciable porosity and internal structure of the oxide film. We also demonstrate that proton transport within the oxide film is slow and leads to a further delay in the microsensor response to pH changes.

EXPERIMENTAL SECTION

Reagents. Nanopure water was obtained using a three-cartridge Millipore purification system. Silver electrodeposition was carried out using a silver plating solution from Transene Co.. Potassium chloride, sulfuric acid (reagent grade), hydrogen peroxide (30%), perchloric acid (70%), acetone (reagent grade), and potassium carbonate were supplied by EM Science. Lithium perchlorate (99.99%), oxalic acid (99%), and silver nitrate were supplied by Aldrich. Iridium (IV) chloride (99.95%) was supplied by Alfa Aesar. Negative photoresist, SU-8 2 was supplied by MicroChem. All chemicals were used as received.

Device Design, Fabrication and Assembly. Figure 2 shows a schematic of the device design. There are six electrodes on a typical device. The far left contact pad, labeled R, leads to a large silver-plated reference electrode. The two counter electrodes (C) are externally shorted to ensure a symmetric current distribution and, thus, ion flux on both sides of the generator electrode (G). There are two identical sensor electrodes (S) flanking the generator electrode. In each experiment, the potential of only one of these electrodes is monitored. The P-ETOF devices were fabricated utilizing photolithographic patterning and physical vapor deposition techniques (lift-off technology). Lithographic microfabrication involves standard, chromic acid-cleaned, 1-in. × 3-in. × 1-mm glass microscope slides. These are spin-coated with Shipley 1818 photoresist and then exposed to pattern the electrodes. After developing and drying, 8−10 nm of chromium and then ~100 nm of gold are deposited via resistive heating evaporation in a vacuum. The slides are then placed in an acetone bath that removes the remaining photoresist and gold, leaving only the electrode assembly behind. A layer of epoxy-based photoresist polymer (SU-8 2) is spun, baked, and exposed to create an insulating layer that separates the working electrode area from the contacts, as shown in Figure 2 by the shaded rectangle over the electrodes. This defines the length of microband electrodes and protects the contact area from further chemical modification. The active electrode length (l) was 2.0 mm. It was selected to be large relative to the width of the interelectrode gap in order to render radial diffusion contribution to the total ion flux at the tip of the generator microelectrode negligible. The area outlined by the dotted line indicates the approximate area confined by the cover slip used as the upper barrier of the thin layer cell shown in Figure 1. The cell height is controlled with the polymeric spacers deposited in the corners of the cover slip.

After device fabrication, the electrodes were chemically modified for use as specific ion generator and sensor pairs. For the Ag^+/Ag system, silver is electroplated from a commercial silver-plating solution on both the G and S microelectrodes. A typical thickness of the silver layer, measured with a stylus profilometer, is ~0.7 μm on the generator and tens of nanometers on the sensor. Chloride P-ETOF experiments required Ag/AgCl electrodes. These were made by oxidizing silver in 0.1 M KCl solutions. The generator electrode is formed by applying a constant anodic current of 1 μA for a period of time sufficient to oxidize approximately three-quarters of the 1.5−2.5 μm thick silver film to AgCl. The preparation of the Ag/AgCl sensors is discussed in the Results and Discussion Section. In the case of proton P-ETOF, the Au generator electrode is left unmodified, and an iridium (IV) oxide layer of 40−250 nm is formed by electrochemically induced precipitation from an alkaline solution containing an iridium oxalate complex following the procedures of Yamanaka.[27] The latter solution was 4 mM $IrCl_4$ with a 10-fold excess of oxalic acid. The pH of the solution was adjusted to 10.5 with K_2CO_3. The resulting solution was allowed to stabilize over 2 days at room temperature. The electrochemically induced deposition was carried out galvanostatically with i = 35 mA/cm^2. In all cases, the values of the Nernstian slopes of the microsensors were determined experimentally. All experiments were carried out in 1 M lithium perchlorate electrolyte. This high concentration of the supporting electrolyte is used to eliminate ohmic potential drop within the narrow channel. The effects of a potential field gradient and migration on the $E-t$ transients were discussed in an earlier report.[19] Initial concentration of the primary ion of interest was set with standard solutions of silver nitrate, potassium chloride, and perchloric or sulfuric acid. A typical P-ETOF experiment involves rinsing and air-drying the electrode assembly, then dropping a few hundred microliters of a desired electrolyte

(27) Yamanaka, K. *Jpn. J. Appl. Phys.* **1989**, *28*, 632.

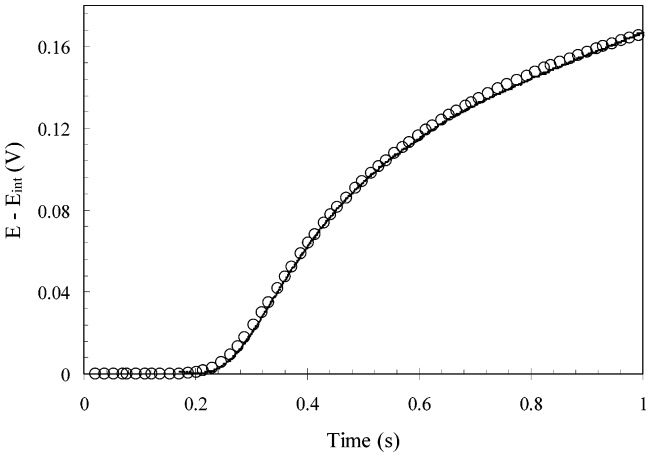

Figure 3. A comparison of the experimental (small dots) and the calculated (open circles) $E-t$ transients of a Ag^+ ETOF experiment obtained under the following experimental conditions: $i_{gen} = 1.0 \times 10^{-5}$ A, $[Ag^+]_{init} = 1.0 \times 10^{-5}$ M, $h = 2.7$ μm, $g = 100$ μm, and $D_{Ag^+} = 1.2 \times 10^{-5}$ cm^2/s.

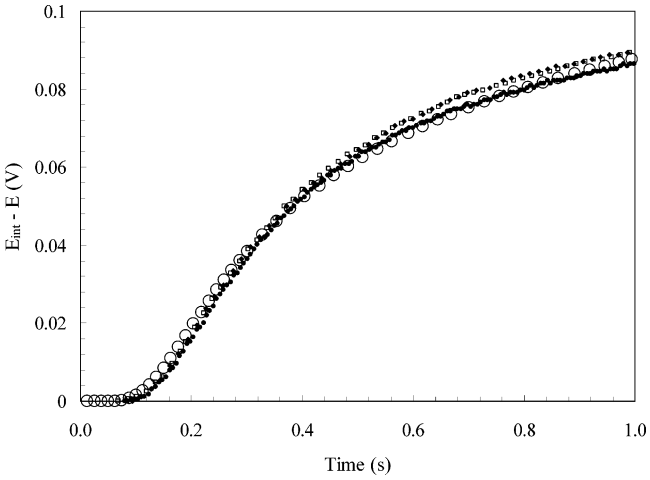

Figure 4. Three $E-t$ transients obtained in the Cl^- ETOF experiments carried out with the same device testing reproducibility of the device assembly process. Open circles represent the theoretical prediction obtained for $i_{gen} = 1.0 \times 10^{-6}$ A, $[Cl^-]_{init} = 1.0 \times 10^{-4}$, $h = 3.3$ μm, $g = 50$ μm, and $D_{Cl^-} = 1.2 \times 10^{-5}$ cm^2/s. The transient obtained in the first, second, and third runs are marked with dots, open squares, and black diamonds, respectively.

solution and closing the cell with the upper cover slip. A small mechanical brace is then used to squeeze the device, immobilize the cover slip, and adjust the thickness of the thin-layer channel. Reproducibility of this step is discussed in the Results and Discussion Section.

Instrumentation. Electrochemical experiments were carried out using a CH Instruments model 660B electrochemical analyzer. Recording of P-ETOF transients is made possible through dual-channel recording during chronopotentiometric experiments. The generator is directly controlled and the open circuit potential is monitored at the sensor electrode. This instrument has a 1-kHz sampling rate and better than 0.5 mV resolution.

Computations. The theoretical $E-t$ transients corresponding to those obtained in the P-ETOF experiments were computed (eq 1) using a Matlab software package (version 6.1.0.450 by The MathWorks Inc.).

RESULTS AND DISCUSSION

P-ETOF Device Performance. The shape of the potential-vs-time transients can be computed using eq 1 together with the Nernst equation. The knowledge of the experimentally determined value of the Nernstian slope of the microsensors and the critical dimensions of the P-ETOF devices are also required. The subsequent comparison between the computed and experimental transients was used to assess the performance of the P-ETOF devices. The interelectrode gap (g, taken as the center-to-center distance between the 10-μm-wide microband electrodes), the electrode length, and the thickness of the narrow channel obtained by measuring the thickness of the polymeric spacers (see the Experimental Section) were measured with ca. ±2% precision. Literature values of the diffusion coefficients were corrected for the particular ionic strength of the electrolyte solutions used in the P-ETOF experiments.[19] The general agreement between the theoretical expectations and the experimental data was excellent and typically reflected the ±2% precision of the measurements of the device dimensions. For example, Figure 3 shows the comparison between the computed and recorded $E-t$ transients in a silver ion P-ETOF experiment. In Figure 4, we compare a set of three Cl^- P-ETOF transients recorded with the same device assembled and opened three consecutive times to test the reproducibility of the device channel thickness. The two runs exhibiting small deviations from the theoretical $E-t$ transient computed with a channel thickness of 3.30 μm could be fit with channel thicknesses of 3.25 and 3.35 μm. This corresponds to a ±1.5% error, likely resulting from the changes in the thickness of the polymeric spacers due to solvent swelling or simple wear following multiple uses. The agreement of the experimental $E-t$ transients with the theory shows that the linear diffusion approximation outlined in the Introduction is appropriate. It also shows that, under these conditions, it is reasonable to neglect the finite size of the microsensor electrode. However, the latter assumption does not hold under the conditions of low generator current or low background concentration of the electrogenerated ions. We address this in the next section.

Delayed Response of Microsensors. Consider again the P-ETOF device shown schematically in Figures 1 and 2. Confinement of the microsensor electrode to a small volume of the narrow channel may lead to a situation in which the change of the sensor potential in response to an increase in the concentration of the primary ion diffusing in the channel requires a nonnegligible decrease in the ion concentration in the volume directly above the sensor surface. This then results in a slower increase of the sensor potential relative to a theoretical expectation, or a delay in the $E-t$ transient. Two such cases featuring Ag^+ P-ETOF experiments carried out in the devices with 3.0- and 1.0-mm thick channels are shown in Figure 5. In these experiments, unlike in the Ag^+ P-ETOF experiment of Figure 3, the generator current is significantly lower. This results in a delayed response of the microsensor (circles) relative to the theoretical expectations (continuous line). Furthermore, the delay observed in the 1-μm channel device is greater than that in the 3-μm-thick channel device. Clearly, in the process of reaching equilibrium, some Ag^+ ions must be reduced at the microsensor surface. This causes their concentration in the small volume of solution in the vicinity

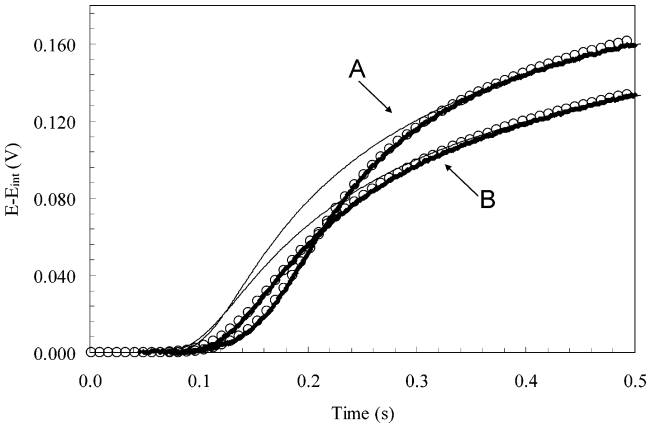

Figure 5. Two experimental Ag^+ ETOF $E-t$ transients (black dots) recorded with the $h = 1.0$ μm (A) and $h = 3.0$ μm (B) devices. The other experimental conditions were $i_{gen} = 1.0 \times 10^{-6}$ A, $[Ag^+]_{init} = 1.0 \times 10^{-5}$, $g = 50$ μm, and $D_{Ag^+} = 1.2 \times 10^{-5}$ cm^2/s. The transients obtained on the basis of eq 1 are shown by a thin, continuous line. The transients marked with open circles were obtained by taking into consideration the finite value of the capacitance of the microsensors of 30 (A) and 31 μF/cm^2 (B).

of the sensor to be actually smaller than expected when only the rate of their diffusive transport is considered (eq 1) and results in a slower increase of the sensor potential.

To quantify this effect, it is necessary to relate the differential mole quantity of the reduced silver ions (dN) to the differential change of sensor potential (dE), its specific capacitance (C_{dl}) and its surface area (A).[19]

$$dN = \frac{C_{dl}(E)A\ dE}{nF} \qquad (2)$$

In general, delays due to the finite size and capacitance of potentiometric sensors must be expected when the supply of the ions participating in a sensor equilibrium reaction is small relative to the demand for their reduction. Indeed, the analogy to the market supply and demand equilibrium is quite appropriate. In the present example, the supply of silver ions can be expressed by the instantaneous flux of electrochemically generated Ag^+ ions at the sensor. In view of eq 1, it is primarily determined by the rate of their generation (i_{gen}). It also inversely depends on the interelectrode gap. Demand refers to the number of moles of silver ions, N, that must be reduced to increase the sensor potential by a certain value, as shown by eq 2. Capacitance is the proportionality constant in this equation. It is important to note that, in view of the Nernst equation, the magnitude of the sensor potential change per decade change of the concentration of the primary ion is constant. Thus, for a given flux of silver ions in the device, the change of the sensor potential and, thus, the demand depends on the initial (background) Ag^+ concentration. When the latter is low, even a small flux of silver ions may require a large change of sensor's potential. This is when demand is likely to exceed supply and a delay in the sensor's response is to be expected. We stress that the observed capacitive delay in the response of the silver microsensor is not at all related to the intrinsic kinetics of this sensor response. In our earlier report, the latter was estimated to be >80 V/s, a value far exceeding the theoretically expected rate of the Ag sensor potential change (continuous lines in Figure 5).[15]

The transient delay phenomenon can be used to deduce the capacitance of the sensor. This is done by fitting the recorded $E-t$ curves using eq 1 and taking into account the finite size and the capacitance of the microsensor. Briefly, the numeric routine developed for this purpose calculates the increments of Ag^+ concentration, ΔC, in the small volume of the solution, v, above the microsensor ($v = wlh$; see Figures 1 and 2) occurring over the arbitrarily small time increments, Δt, using eq 1. We then assume that the silver ions contained in the volume of the solution directly above the microsensor are in the Nernstian equilibrium with the sensor. This requires an iterative computation of the true equilibrium concentration of silver ions and the corresponding sensor potential that takes into account the fact that some quantity of silver ions (N) must be reduced to adjust the sensor potential to the true equilibrium value, as dictated by eq 2. Clearly, the true equilibrium Ag^+ concentration is smaller than that obtained when only diffusion is considered. Likewise, the true equilibrium potential of the sensor is also smaller and rises less rapidly. The sensor's intrinsic capacitance is the only adjustable parameter. It is assumed to be constant over the range of the sensor potentials recorded in a transient. Two such fits are shown in Figure 5 as heavy continuous lines. The value of C_{dl} obtained in this way for several different Ag^+ P-ETOF devices operated under different conditions, 31 ± 2 μF/cm^2, is in excellent agreement with the capacitance found for the same silver microelectrodes using fast scan cyclic voltammetry in a 0.1 M KNO_3 solution. In the data analysis procedure outlined here, C_{dl} was a single adjustable parameter. We knew the diffusion constant of silver ions. If the latter were not available, it would be, in fact, possible to simultaneously determine both D and C_{dl} by relying on a nonlinear least-squares analysis; however, this approach is less precise than an alternative scheme in which D is determined first in an experiment run under conditions of a negligible capacitive delay (high generation rate and high initial concentration of the primary ion). Knowing D, one can then more precisely determine C_{dl} of a sensor, as shown in Figure 5. We also point out that the assumption of Nernstian equilibrium adopted in that case may not hold for all potentiometric microsensors. As shown below, an iridium oxide pH sensor is one such case.

Capacitance of the Silver/Silver Chloride Microsensors. Next, the same approach was used to measure the capacitance of the Ag/AgCl microsensors. AC impedance investigations of the interfacial properties of the Ag/AgCl in chloride electrolytes have been reported, for example, by Buck and co-workers.[28] The response of this system to an ac perturbation is rather complex and requires a multicomponent equivalent circuit to interpret the data. In fact, Buck's analysis of the impedance data does not yield a parameter that is equivalent to the interfacial capacitance, which we could then compare to our measurements reported below.

In the Cl^- P-ETOF experiments, both the generator and sensor microelectrodes were produced by first electroplating gold substrates with silver, followed by its partial oxidation in a 0.1 KCl electrolyte, as described in the Experimental Section. The thickness of the silver films deposited on generator microelectrodes was large, 1.5−2.5 μm. Following its oxidation to silver chloride,

(28) Rhodes, R. K.; Buck, R. P. *Anal. Chim. Acta* **1980**, *113*, 55−66.

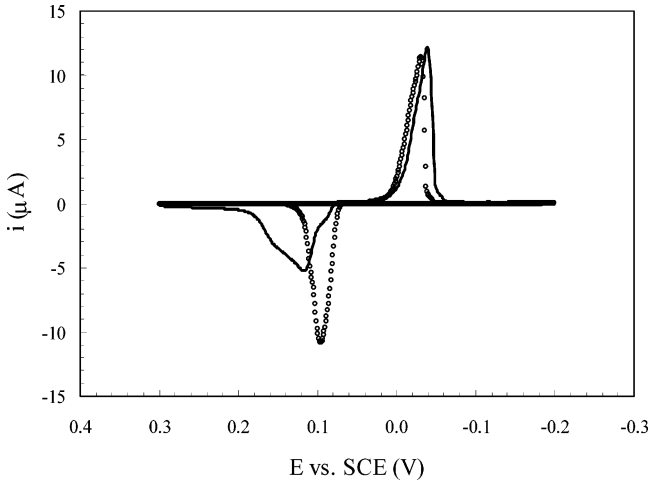

Figure 6. The first (solid line) and the fourth (open circles) continuous sweep cyclic voltammograms recorded with a microband electrode coated with a 100-nm-thick Ag film in a 0.10 M KCl solution; $v = 10$ mV/s; $E_{init} = -0.2$ V vs SCE.

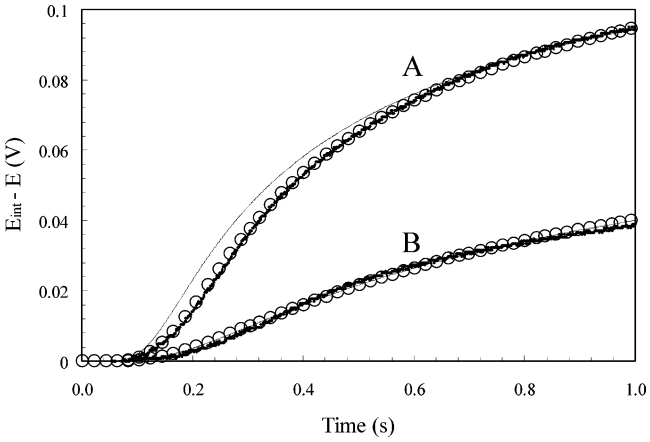

Figure 7. Two experimental Cl^- ETOF $E-t$ transients (black dots) recorded in a device with $[Cl^-]_{init}$ of 1.0×10^{-4} M (A) and 1.0×10^{-3} M (B). The chloride ion microsensors were prepared using method 4. The other experimental conditions were $i_{gen} = 1 \times 10^{-6}$ A, $g = 50$ μm, $h = 3.0$ μm, and $D_{Cl^-} = 1.2 \times 10^{-5}$ cm^2/s. The theoretically calculated transients were either obtained on the basis of eq 1 (thin, continuous lines) or were computed using the iterative algorithm (open circles) with the capacitance of the microsensors of 140 μF/cm^2.

the generator electrode could accommodate current pulses as high as 50 mA/cm^2 to generate chloride ions. Preparation of the Cl^- sensor microelectrodes required thinner, 20−100-nm-thick silver films. These then served to form Ag/AgCl microsensors using one of the following four methods devised to examine the dependence of the sensor capacitance on the thickness of the silver chloride film and the roughness of the silver surface.

Method 1. This method did not involve any deliberate electrochemical oxidation of silver substrate; however, using chronopotentiometry with $i = 10^{-7}$ A, we determined that the charge due to AgCl reduction spontaneously formed on the silver microsensor following its exposure to 0.1 M KCl is 250−500 μC/cm^2. This corresponds to approximately a monolayer quantity of AgCl. Similar results were obtained for the sensors produced by method 3, below.

Method 2. Silver film was electrooxidized in a single voltammetric sweep in 0.1 M KCl solution, and the electrode was disconnected or brought to an open circuit at the positive potential limit. The current−voltage curves recorded in such experiments are shown in Figure 6. The shape of these voltammograms suggests that essentially the entire silver film is converted to AgCl. However, integration of the oxidation current and comparison of the anodic charge with the charge due to electrodeposition of the silver film shows that only 85 ± 8% of the originally electrodeposited silver is converted to silver chloride. We hypothesize that the remaining silver is either insulated by the AgCl film or becomes trapped as small particles within the AgCl layer during the oxidation process.

Method 3. The electrooxidation and silver redeposition cycle was carried out at least three or four times, or until a steady-state voltammogram was reached. The latter is also shown in Figure 6. The last of these cycles was stopped, and the electrode was disconnected at the negative potential limit.

Method 4. Following the potentiostatic cycling of method 3, the last cycle was stopped, and the electrode was disconnected at the positive potential limit. The charge under the anodic branch of the current is ∼34% smaller than that obtained by the integration of the first cycle in Figure 6 and corresponds to only ∼58% of the charge due to the initially electrodeposited silver. Clearly, voltammetric cycling of the silver film microelectrodes in 0.1 M KCl described here further increases the fraction of electrochemically inactive silver. The open circuit potential of the sensors produced by methods 2 and 4 (with thick AgCl coatings) in 0.1 M KCl was typically +0.05 V vs SCE. In the same electrolyte, the microsensors produced by methods 1 and 3 (carrying only approximately monolayer films of AgCl) exhibited an open circuit potential of −0.1 and −0.05 V, respectively.

Typical Cl^- time-of-flight $E-t$ transients are shown in Figure 7. They were recorded using the same value of the generator current of 1.0 μA with the background KCl concentration of 1.0 and 0.10 mM. As expected, the transient recorded in the low background chloride concentration exhibits a capacitive delay. Fitting those types of transients yielded the microsensor's capacitance of 100 ± 10, 100 ± 10, 130 ± 10, and 140 ± 10 μF/cm^2 for the microsensors obtained by methods 1 through 4, respectively. The second $E-t$ transient in Figure 7 did not exhibit capacitive delay. Nevertheless, when the same value of the capacitance that resulted in the agreement between theory and experiment of transient A is used to compute transient B, its shape overlays that obtained using eq 1. Considering all these results, one observes that, most conspicuously, the capacitance of the Ag/AgCl sensors (in ∼1 mM KCl, 1.0 M $LiClO_4$) is at least three times larger than that of a silver electrode measured in the same electrolyte not containing chloride ions. Next, we note that the thickness of the electrodeposited silver chloride film does not affect the capacitance of the system, as evidenced by the data for method 1 vs method 2. This is consistent with the fact that AgCl films are rather porous and easily permeable to the external electrolyte. However, potentiostatic cycling does increase the interfacial capacitance by ∼30%. In the case of the sensor produced by method 3, this finding can be easily explained by a larger surface area of the silver film. It is well-known that the type of potentiostatic cycling used here does result in an increased roughness of the silver.[29,30] The fact that the sensor obtained by

(29) Jeanmaire, D. L.; Van Duyne, R. P. *J. Electroanal. Chem.* **1977**, *84*, 1−20.

method 4 has even higher capacitance reflects perhaps the increasing fraction of the metallic silver trapped as small particles in a spongy film of silver chloride and the resulting changes of the film dielectric properties. As pointed out above, the Ag/AgCl capacitance data have never been reported before. To the best of our knowledge, the P-ETOF method is uniquely capable of yielding such data.

Iridium Oxide Microsensors. As mentioned previously, iridium oxide films formed by electrochemically induced precipitation (see the Experimental Section) show promise as a micropotentiometric pH sensors.[5,6,27,31−38] We assessed their general electrochemical behavior and the kinetics of their response in our previous report.[15] Although the exact mechanism of their functioning remains one of speculation, the stability and sensitivity make this material well worth further investigation. Like the silver and chloride systems reported above under conditions of low availability of the primary ion, considerable delays in $E-t$ can also be observed in the proton P-ETOF experiments. Furthermore, the delays in the response of the iridium oxide sensors show a strong correlation with the oxide film thickness.

Figure 8 shows the $E-t$ transients recorded with the oxide films of three different thicknesses ranging from 120 to 230 nm. The other experimental conditions were the same in all cases and were selected to result in delayed $E-t$ transients. Unlike the silver and silver chloride sensors, iridium oxide layers show $E-t$ transients that cannot be fit with a single capacitance value over the entire time span covered in these experiments. The fits shown in Figure 8 were aimed to match the experimental transients at longer times. Consequently, convergence of the experimental and calculated curves is observed at times >0.3, 0.5, and 0.6 s for the microsensors with IrO_2 films of 120, 170, and 230 nm, respectively. The corresponding capacitance values found to fit the data were 400, 800, and 1300 μF/cm^2. To fit the entire $E-t$ transients, we would have to introduce time- or potential-dependent capacitances with their initial values exceeding those listed above by at least 2 orders of magnitude. We judged such an approach unjustified and unrealistic. The capacitance values given above are significantly greater than those seen for the other sensors, most likely due to the highly porous nature of the anodically deposited iridium oxide layers.[39,40] In fact, the capacitances of the IrO_2 films obtained in the H^+ P-ETOF experiments correlate reasonably well with the film thickness, as shown in Figure 9, yielding specific capacitance of 59 ± 6 F/cm^3. This correlation notwithstanding, we do not fully understand the initial delay or an apparent induction period observed in the pH response of the IrO_2 sensors in Figure 8. Our previous work has shown that these oxide films exhibit the maximum rate of response of ~34 V/s.[15] Therefore, it is not likely that the initial induction time or slow response is due to slow kinetics of proton transport within the oxide film or slow proton

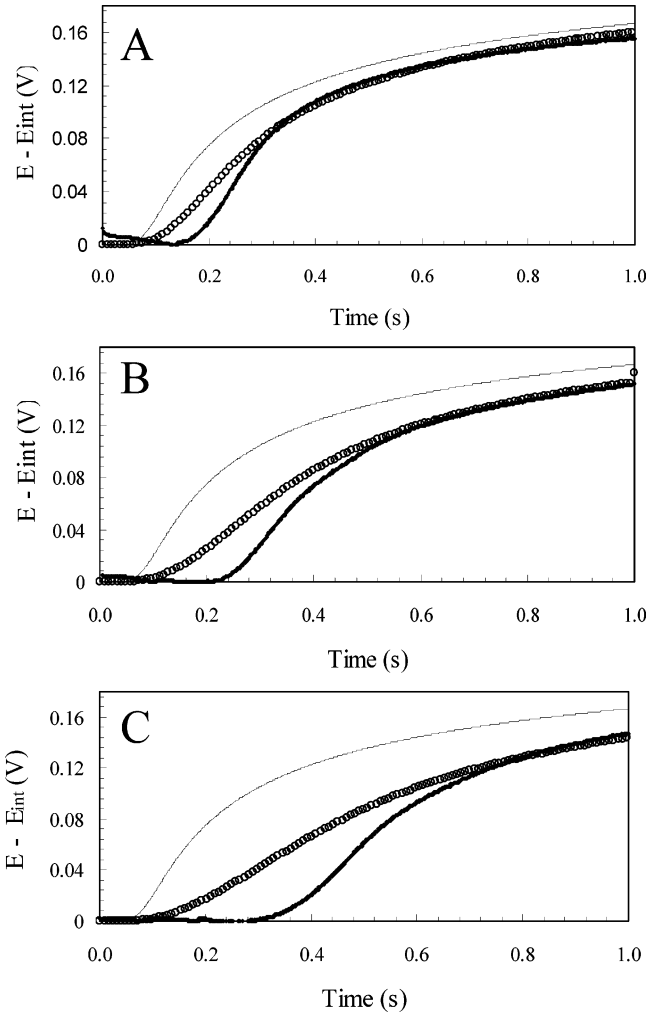

Figure 8. Three H^+ ETOF $E-t$ transients (black dots) recorded with the IrO_2 pH microsensors of 120 (A), 170 (B), and 230 nm (C) in thickness. The other experimental parameters were $i_{gen} = 5.0 \times 10^{-6}$ A, $[H^+]_{init} = 0.1$ mM, $h = 3.0$ μm, $g = 100$ μm, and $D_{H^+} = 7 \times 10^{-5}$ cm^2/s. The transients computed using eq 1 are marked with thin continuous lines, and those obtained using the iterative algorithm with the capacitance of the microsensors of 400 (A), 780 (B), and 1300 μF/cm^2 (C) are marked with open circles.

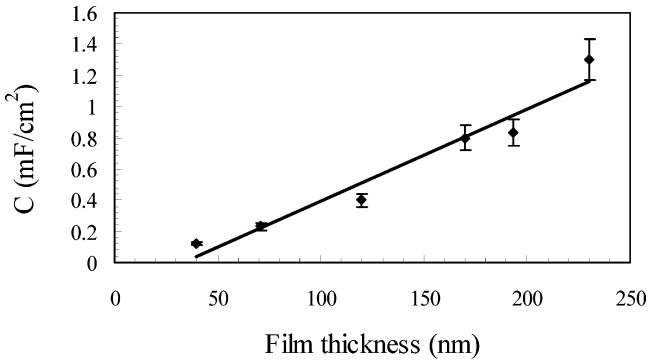

Figure 9. A plot of the capacitance of IrO_2 microsensors as a function of the IrO_2 film thickness. The error bars correspond to ca. ±10% standard deviations of the capacitance values obtained by fitting ETOF $E-t$ transients, such as those in Figure 8.

(30) Schultz, S. G.; Janik-Czachor, M.; Van Duyne, R. P. *Surf. Sci.* **1981**, *104*, 419−434.
(31) Katsube, T.; Lauks, I.; Zemel, J. N. *Sens. Actuators* **1982**, *2*, 399.
(32) Yuen, M. F.; Lauks, I.; Dautremont-Smith, W. C. *Solid State Ionics* **1983**, *11*, 19.
(33) Burke, L. D.; Mulcahy, J. K.; Whelan, D. P. *J. Electroanal. Chem.* **1984**, *163*, 117
(34) Fog, A.; Buck, R. P. *Sens.ors and Actuators* **1984**, *5*, 137.
(35) Hitchman, M. L.; Ramanathan, S. *Analyst* **1988**, *113*, 35.
(36) Glab, S.; Hulanicki, A.; Edwall, G.; Ingman, F. *Crit. Rev. Anal. Chem.* **1989**, *21*, 29.
(37) Baur, J.; Spaine, T. W. *J. Electroanal. Chem.* **1998**, *443*, 208.
(38) Wang, M.; Yao, S.; Madou, M. *Sens. Actuators, B* **2002**, *81*, 313.
(39) Petit, M.; Plichon, V. *J. Electroanal. Chem.* **1998**, *444*, 247.
(40) Mo, Y.; Stefan, I. C.; Cai, W.-B.; Dong, J.; Carey, P.; Scherson, D. A. *J. Phys. Chem. B* **2002**, *106*, 3681.

interaction at the internal oxide/solution interfaces. We hypothesize that this rather large induction time could be perhaps explained by pH-induced morphological changes of the film structure, such as swelling or film expansion.

CONCLUSIONS

Our electrochemical time-of-flight technique utilizes photolithographically prepared dual-microband devices to generate $E-t$ transients that we can use to characterize the response time and the capacitance of various sensors. The development of silver ion, chloride, and proton generator/sensor systems is described. The results show excellent agreement between the measured $E-t$ transients and those obtained theoretically on the basis of diffusion equations and the experimentally determined Nernstian slopes of the microsensors whenever the size of the microsensor and, thus, its capacitance can be assumed to be negligible. In other cases, when this assumption cannot be made, slower rising $E-t$ transients are recorded. Using an iterative numerical algorithm, these delayed transients can be interpreted to yield the sensor's capacitance. Results for the three systems mentioned above are presented. The capacitances derived from this method agree well with those measured by fast scan voltammetry for the simple silver system. It also gives consistent results for the silver/silver chloride system in which AC impedance does not. Finally, in the case of porous iridium oxide pH sensors, our P-ETOF method shows the dependence of the sensor's capacitance on the thickness of the oxide films, yielding a specific capacitance of ~60 F/cm^3. We also observed that these pH sensors exhibit an additional delay or an induction time that cannot be accounted for by the sensor's capacitance and that continues to be a subject of our ongoing investigations.

ACKNOWLEDGMENT

This work was supported by the National Science Foundation under Grants CHE-0416349. We also acknowledge the donors of the Petroleum Research Fund, administered by the American Chemical Society, for partial support of this research and a Fulbright Fellowship Grant to E.H. administered by the Polish–U.S. Fulbright Commission.

Received for review March 10, 2006. Accepted June 30, 2006.

AC060449W